Frequency response functions and modal parameters of a rotating system exhibiting rotating damping

B.Vervisch [1,2], **S.Derammelaere**[1], **K.Stockman** [1], **M.Loccufier** [2]
[1] University of Ghent, Department of Industrial Systems and Product Design,
Graaf Karel de Goedelaan 5, B-8500, Kortrijk, Belgium
e-mail: **bramf.vervisch@ugent.be**

[2] University of Ghent, Departement of Electrical Engineering, Systems and Automation
Technologiepark 914, B-9052, Zwijnaarde, Belgium

Abstract
In the analysis of the stability threshold speed caused by rotating damping in rotating machinery, there is a lack of experimental data. This stability threshold speed can be found theoretically by means of a linear speed dependent model. The accuracy of the model depends highly upon the linearity and especially on the damping type that has been chosen. In this paper, an experimental setup is presented which was designed to verify the theoretical modeling of rotating damping and its destabilizing effect. A rotating shaft is used to extract frequency response functions at different speeds. The shaft is excited with an automated impact hammer and the response is measured by eddy current probes. From these frequency response functions, the poles are extracted and compared to the poles derived from the model.

1 Introduction

In rotating machinery, damping plays an important role in the stability analysis. Besides dissipating energy, damping can cause a transformation of rotational energy into a whirling motion also called self-excited vibrations [1]. The mechanism that causes this destabilizing effect is rotating damping or rotor internal damping [2]. By modeling the rotor using a linear speed dependent model this rotating damping can be included as a speed dependent effect. Together with the gyroscopic effect it causes the system poles to be speed dependent. Typically, in rotordynamics, the poles are plotted in function of the rotating speed. The imaginary parts are plotted in the Campbell diagram and the real parts in the decay rate plot [3]. In order for the rotor to be stable, the real parts of the poles have to be negative. Whenever one of the poles has a positive real part, instability occurs. The rotating speed at which this instability occurs, i.e. the stability threshold speed, mainly depends on the ratio between the rotating damping and the non-rotating damping. It has been shown theoretically that it is impossible to rotate above the stability threshold speed [4]. However, these conclusions are generally based on a theoretical damping model wich assumes a linear behavior [5][6]. Whether these assumptions hold can only be validated by experimental data. In literature there is a lack of these experimental validations. Therefore, this paper focuses on the possibility to extract the poles from a rotating system and discusses the usefulness of these measurements. A test bench is constructed containing a long thin shaft that is placed on two angular contact spindle bearings at both ends. This yields reduced bearing effects as clamped boundary conditions are approximated. The shaft is also modeled with finite elements such that frequency responses can be simulated at different speeds together with the Campbell diagram and the decay rate plot. The simulations and measurements are compared. Because the system is rotating, conventional measurement techniques are insufficient. The excitation is performed by a remotely controlled hammer system. This excitation mechanism allows safe and reproducible measurements. The responses are measured by eddy current probes. This contribution initiates an experimental technique to identify the damping matrix

of a rotating system. In section two, the instability caused by rotating damping is discussed theoretically, the stability threshold speed is derived and the used damping model is discussed. Section three describes the rotating damping setup and what design decisions are made. Section four discusses the measurement procedure that is used. In section five the resulting frequency response functions and Campbell and decay rate plot are presented and discussed.

2 Instability in rotating machinery caused by rotating damping

Instability in rotating machinery caused by rotating damping can be described by means of a linear speed dependent model. Both the linear speed dependent model and the physical mechanism that causes instability are decribes. Within this linear model, the stability threshold speed can be calculated by deriving the system poles. The dependency of the parameters is discussed.

2.1 The linear speed dependent model

The model used in this paper is linear and discretized by means of finite elements. The equations of motion contain a mass matrix, $\mathbf{M}$, a damping matrix, $\mathbf{C}$, and a stiffness matrix, $\mathbf{K}$. Due to rotation, some of these properties can change periodically in time, thus, the matrices become time dependent [7].

$$\mathbf{M}(t)\ddot{\mathbf{q}} + \mathbf{C}(t)\dot{\mathbf{q}} + \mathbf{K}(t)\mathbf{q} = \mathbf{f}(t), \quad \mathbf{q}(t), \mathbf{f}(t) \in \mathbb{R}^n \tag{1}$$

with n, the degrees of freedom. A majority of rotating machinery contains only isotropic rotating elements with time invariant properties. Under these assumptions, only the rotating speed Ω will affect the matrices:

$$\mathbf{M}(\Omega)\ddot{\mathbf{q}} + \mathbf{C}(\Omega)\dot{\mathbf{q}} + \mathbf{K}(\Omega)\mathbf{q} = \mathbf{f}(t), \quad \mathbf{q}(t), \mathbf{f} \in \mathbb{R}^n \tag{2}$$

The most important effects causing this speed dependency are the gyroscopic effect and rotating damping. Throughout this paper only rotating effects such as the gyroscopic effect and rotating damping are accounted for. The external forces are considered to be zero. Therefore, when using a real coordinate system, the linear speed dependent model in (2) can be

$$\begin{bmatrix} \mathbf{M} & \mathbf{0} \\ \mathbf{0} & \mathbf{M} \end{bmatrix} \ddot{\mathbf{q}} + \left(\begin{bmatrix} \mathbf{C}_n + \mathbf{C}_r & \mathbf{0} \\ \mathbf{0} & \mathbf{C}_n + \mathbf{C}_r \end{bmatrix} + \Omega \begin{bmatrix} \mathbf{0} & \mathbf{G} \\ \mathbf{-G} & \mathbf{0} \end{bmatrix} \right) \dot{\mathbf{q}} + \left(\begin{bmatrix} \mathbf{K} & \mathbf{0} \\ \mathbf{0} & \mathbf{K} \end{bmatrix} + \Omega \begin{bmatrix} \mathbf{0} & \mathbf{C}_r \\ \mathbf{-C}_r & \mathbf{0} \end{bmatrix} \right) \mathbf{q} = \mathbf{0} \tag{3}$$

with $\mathbf{G}$ and $\mathbf{C}_r$ respectively the gyroscopic matrix and the rotating damping matrix and $\mathbf{C}_n$ the non-rotating damping matrix. The gyroscopic effect and the rotating damping are influenced by the rotating speed and generate an asymmetry into the system. Classical modal analysis techniques, that mostly assume symmetric matrices, become insufficient. The rotating speed dependency in these matrices has an influence on the system poles. Not only the imaginary part of the poles, i.e. the whirling speed, becomes speed dependent, but also the real part. When the real part has a negative sign, vibrations die out in time. When it becomes positive, there is an exponential growth of the vibrations or an instability.

If complex coordinates are used [3], equation (3) reduces to

$$\mathbf{M}\ddot{\mathbf{z}} + \left(\mathbf{C}_n + \mathbf{C}_r - i\Omega\mathbf{G}\right)\dot{\mathbf{z}} + \left(\mathbf{K} - i\Omega\mathbf{C}_r\right)\mathbf{z} = 0 \tag{4}$$

where $\mathbf{z}$ is a vector containing complex coordinates. By using complex coordinates the degrees of freedom of the system are reduced and all matrices become symmetric. A drawback is that the results are not that easy to interpret physically.

2.2 Instability due to rotating damping

In vibrating structures, the role of damping is to dissipate energy caused by vibration. Dominant vibrations in a rotor are caused by its natural frequencies and forced vibrations such as unbalance, misalignments, machine faults, ... Damping in rotors can be located in non-rotating parts, mainly bearings, and into rotating parts such as shrink fits, seals or material damping of the rotor itself. This type of damping is called rotating damping and can cause instability. Instead of dissipating vibrational energy into heat, it transforms into whirling energy causing unwanted motion. The whirling speed ω does not have to coincide with the rotating speed Ω. In Figure 1 the section of a shaft is depicted for three different situations: one synchronous whirl in Figure 1b, with $\Omega = \omega$, and two asynchronous whirls, i.e. $\Omega < \omega$ in Figure 1a and $\Omega > \omega$ in Figure 1c. The damping force occurring in these three situations depends on how the material is undergoing a change. In linear theory, the damping force from a stress-strain relation is proportional to the strain rate of change [8][2], or how the strain of the material is changing at a certain location as a function of time. In Figure 1 a shaded marker is symbolizes the movement of the shaft material. A red dot on the shaft represents compression and blue represents stretching. First, if $\Omega < \omega$, the rotating speed lags the whirling motion stretching the material at the shaded marker in t_1 and traveling to compression at t_4. The strain rate of change opposes the whirling speed and a damping force occurs opposed to the whirling. It reduces the whirling amplitude,. Second, if $\Omega = \omega$, the shaft bends once and then remains in its initial state, so the strain rate of change is zero. As a result, the damping force is zero. Third, if $\Omega > \omega$, the rotating speed leads the whirling motion, material at the shaded marker is traveling from compressed to stretched in the same direction of the whirling speed. This leading results in damping that enforces the whirling speed: the system becomes unstable. In conclusion, when passing a whirling speed, a sign change occurs in the damping and instability occurs if no other damping forces are present.

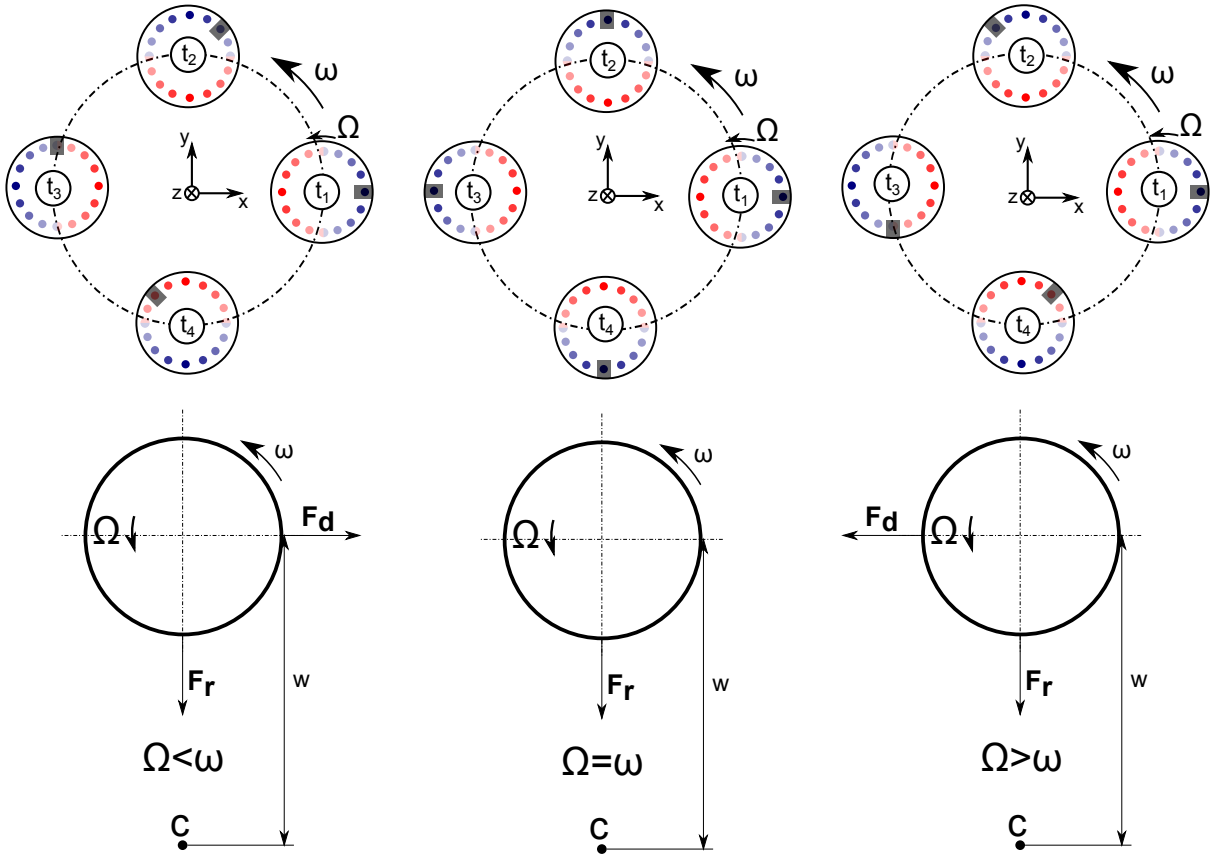

(a) Rotating speed < whirling speed (b) Rotating speed = speed (c) Rotating speed > whirling speed

Figure 1: Section of a shaft that is exposed to whirling

2.3 Proportional damping

The damping matrices can be modeled in a proportional way. Proportional damping is defined as

$$\mathbf{C}_n = a \quad ; \quad \mathbf{K}_b + b\mathbf{M}\mathbf{C}_r = a \quad ; \quad \mathbf{K}_r + b\mathbf{M} \tag{5}$$

with $\mathbf{K}_b$ containing the stiffness of the bearings and $\mathbf{K}_r$ the stiffness of the rotor. Usually, a damping coefficient is used to define the damping [4][9]. This both leads to matrices proportional to the stiffness matrix only.

$$\mathbf{C}_n = \eta_b \mathbf{K}_b \mathbf{C}_r = \eta_v \mathbf{K}_r \tag{6}$$

with η_b and η_v the viscous loss factor for the bearings and the shaft. It is important to remark that although both the non-rotating damping matrix and the rotating damping matrix are proportional to rotating and non-rotating stiffness matrices, the combined damping matrix is no longer proportional. This leads to complex mode shapes.

2.4 The stability threshold speed

The stability threshold speed can be derived easily if complex coordinates (4) are used [5][6]. Because all matrices are symmetric, decoupling can be implemented. If $\mathbf{q} = \mathbf{z}e^{\mu t}$ is a solution of (4), a quadratic eigenvalue problem is formed [10]. By premultiplying the equations of motion by the complex conjugate eigenvector, n scalar equations are obtained

$$\bar{\mathbf{z}}_i^T \left[\mathbf{M}\mu^2 + (\mathbf{C}_n + \mathbf{C}_r - i\Omega\mathbf{G})\,\mu + (\mathbf{K} - i\Omega\mathbf{C}_r)\right]\mathbf{z}_i = \mathbf{0} \tag{7}$$

The equations are of the form

$$m_i\mu_i^2 + (c_{ni} + c_{ri} - i\Omega g_i)\,\mu_i + k_i - i\Omega c_{ri} = 0 \tag{8}$$

$\mathbf{z}$ is defined by an arbitrary constant and is chosen such that $\bar{\mathbf{z}}_i^T\mathbf{M}\mathbf{z}_i = m_i = 1$. Due to the matrix properties the scalars c_{ni}, c_{ri}, g_i and k_i are all real and positive

$$\bar{\mathbf{z}}_i^T\mathbf{K}\mathbf{z}_i = k_i > 0 \tag{9}$$
$$\bar{\mathbf{z}}_i^T\mathbf{C}_r\mathbf{z}_i = c_{ri} \geq 0 \tag{10}$$
$$\bar{\mathbf{z}}_i^T\mathbf{C}_n\mathbf{z}_i = c_{ni} > 0 \tag{11}$$
$$\bar{\mathbf{z}}_i^T\mathbf{G}\mathbf{z}_i = g_i \geq 0 \tag{12}$$
$$\tag{13}$$

In order to find the stability threshold, the real part of μ_i has to become positive. This happens at a rotating speed Ω_{si}

$$\Omega_{si} = \omega_{si}\left(1 + \frac{c_{ni}}{c_{ri}}\right) \tag{14}$$

and a corresponding whirl speed, ω_{si} is

$$\omega_{si} = \pm\sqrt{\frac{k_i}{1 - g_i\left(1 + \frac{c_{ni}}{c_{ri}}\right)}} \tag{15}$$

From equation (14) and inequalities (10) and (11) it is clear that the sign of Ω_{si} is always the same as the one of ω_{si}. Moreover, the sign of Ω_{si} is a convention chosen by the user and here positive. This means that in (15) only the positive ω_{si} is an existing solution meaning the stability threshold speed is a forward whirling speed. It can be concluded that all backward modes are stable. Furthermore, because there are 4n eigenvectors, there are 4n equations like (8), each with their own quantities (9-12) such that every mode has a potential stability threshold speed. Nevertheless, it is shown that it is impossible to rotate above a stability threshold [4]. As a result, there is only one threshold, the lowest value of (14).

Analyzing (14) and (15) shows that the relation between the parameters c_{ni} and c_{ri} is important in stability calculations. If the parameter c_{ni} is much higher than c_{ri}, the stability threshold speed becomes very high and stable rotation can be secured for a large speed range. On the other hand, a high c_{ri}/c_{ni} ratio leads to a stability threshold speed that roughly equals the first forward whirling speed. In this case, the range of stable rotation is almost limited to the first whirling speed. An accurate knowledge of c_{ni} and c_{ri} is necessary. However, these parameters are derived from the rotating and non-rotating damping matrix and depend highly on the modeling choice. Therefore an experimental validation is needed.

2.5 Campbell diagram and decay rate plot of parameters

Parameters (9-12) can not only be used to calculate the stability threshold speed, but also to visualize the trend of the poles as a function of the rotating speed. Typically this is done by a Campbell diagram and a decay rate plot. Therefore, (8) is solved for μ

$$\mu = -\frac{c_{ni} + c_{ri} - ig_i\Omega}{2} \pm \sqrt{(c_{ni} + c_{ri} - ig\Omega)^2 - 4\left[k_i - i\Omega c_{ri}\right]} \tag{16}$$

By splitting this into its real and imaginary part, respectively the decay rate plot and the Campbell diagram can be calculated. The real part of the poles, σ, and the imaginary part, ω, can be written as

$$\sigma_i(\Omega) = Re(\mu_i(\Omega)) = -\frac{c_{ni} + c_{ri}}{2} \pm \frac{1}{2}\sqrt{a + \sqrt{\frac{a^2 + b^2}{2}}} \tag{17}$$

$$\omega_i(\Omega) = Im(\mu_i(\Omega)) = \frac{g_i\Omega}{2} \pm \frac{1}{2}sgn(b)\sqrt{-a + \sqrt{\frac{a^2 + b^2}{2}}} \tag{18}$$

With

$$a = (c_{ni} + c_{ri})^2 + g_i^2\Omega^2 - 4k_i \tag{19}$$

$$b = -2g_i\Omega(c_{ni} + c_{ri}) + 4\Omega c_{ri} \tag{20}$$

Because both Campbell diagram and decay rate plot are expressed by the parameters (9-12), they are called the Campbell diagram and the decay rate plot of parameters. By doing this, an easy tool is created for a machine designer to check the influence of each individual parameter on either the whirling speed or the decay rate.

2.6 Possible deviations of the predicted stability threshold speed

The linear speed dependent model creates a transparent way to derive the stability threshold speed and creates an overview of which parameters have the biggest impact. However, a real rotor will deviate from these predictions. The main reasons are nonlinearities and the damping model. As in all real structures, nonlinearites will occur. The damping model used here is proportional to the stiffness matrix. There is no physical evidence that damping would behave this way. Therefore there are other methods to describe the damping. The influence of these nonlinearities and the damping can only be validated by measurements.

3 The rotating damping setup

Creating a test setup that validates the effect of rotating damping is not that obvious. All side effects that could lead to uncertainties should at least be minimized. Typically vibrations caused by the motor, misalignment problems and residual unbalance should be avoided. Second, by constructing a finite element model, insight can be gained into the behavior of the rotating setup. This model should be transparent and build up with elementary equations. All parameters, such as mass, stiffness and boundary conditions have to be known. Also, for practical reasons, the dimensions and the speed range have to be kept low. The main idea is to create a rotating beam clamped on both sides. This means that, theoretically, all influence by the motor is eliminated and the boundary conditions in the model can be achieved very easily (Fig 2). Also it is chosen to keep the gyroscopic effect low.

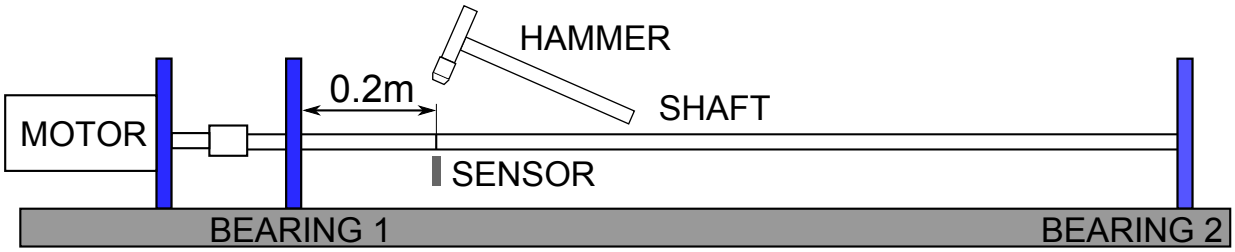

Figure 2: A concept of a rotating clamped beam can eliminate unwanted effects coming from motor and bearings

Achieving these conditions on a practical setup needs some important considerations such as the choice of the bearings and the housing, the motor, and the alignment.

3.1 The motor

The most important property of the motor is the speed range. In order to get a high speed range in a compact motor an electronically commutated motor or a so called brushless DC motor with hall sensors is used. It has a nominal speed of 5490 rpm and a no load speed of 6160 rpm. An encoder is needed to control the speed between 0-1000 rpm, which is a drawback.

3.2 Bearings and housing

The bearings and the bearing housings are critical in this application. If clamped boundary conditions are intended, the bearings and the housing can not allow any translation, nor any rotation. High precision bearings are needed. To prevent the rotating, single row angular contact bearings are chosen, two at each side. They are mounted back-to-back and the outer rings are pushed together to get a stiff arrangement and to avoid tilting. The bearings are FAG B7000-E-2RSD-T-P4S-UL high precision spindle bearings with a contact angle of 25°.They are already lubricated and have a small pretension in order to get this high precision. The housings are massive blocks to obtain the high stiffness. A schematic breakdown view of the mounting is shown in Figure 3

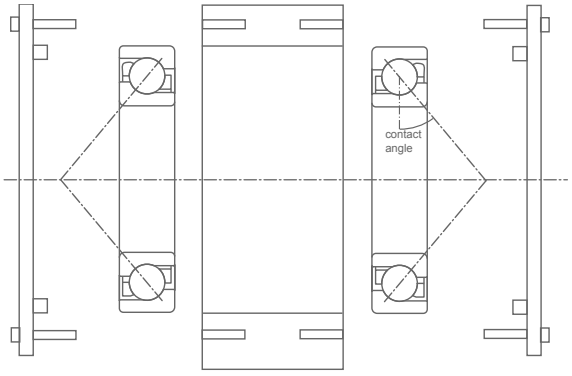

Figure 3: The bearings are arranged back-to-back and mounted in massive blocks to get a high stiffness on translation and rotation

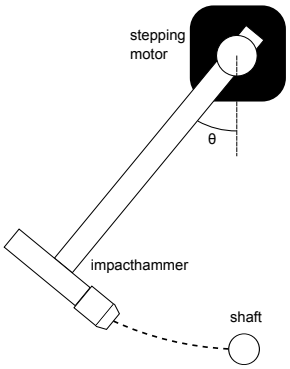

Figure 4: The impact hammer is automatized by means of a small stepping motor in order to get a reproducible impact

3.3 The rotor

For the rotor, a long thin shaft is chosen. In order to avoid unwanted effects, and to focus on the stability threshold, no extra disks are added to the rotor. By doing this, the gyroscopic effect is almost negligible.

A steel shaft is chosen with a diameter of 0.01 m and a length between the bearings of 1.115 m. With the speed range of the motor, it should at least be possible to rotate above the first whirling speed. The boundary conditions created with the bearings will be inbtween clamping and pinning. the first three natural frequencies for these two boundary conditions are given in Table 1. According to these calculations and the motor specifications, rotating above the first natural frequency is possible.

clamped		pinned	
rad/s	rpm	rad/s	rpm
105,8837	1011,115	240,3034	2294,728
423,7493	4046,507	661,9071	6320,747
953,7041	9107,203	1298,067	12395,63

Table 1: Comparison between the undamped natural frequency of the clamped rotor and the pinned rotor

3.4 The alignment

There are two strategies for the alignment. The first strategy is to design a setup that can be aligned very easily so that it is possible to align it with laserequipment. However, these kind of alignment techniques are time consuming and always result in some residual misaligment. In this paper the rotor is build upon a length measurement test bench and the components are constructed such that a high precision alignment is created in the construction phase The major drawback of this strategy is that any errors create residual misalignment, but this misalignment can be reproduced throughout every measurement.

3.5 The impact hammer

The determination of the frequency response functions in experimental modal analysis requires a known excitation. There are several excitation techniques possible such as an electrodynamic shaker, a hammer and more specialized techniques such as pressurized air, acoustics or laser. The properties are summed up in Table 2. An electrodynamic shaker on a rotating setup would require a dedicated bearing on the location of excitation. Even if it was chosen to put this in a node of a mode shape, this would still influence the measurement too much by adding mass, stiffness and damping. Pressurized air and acoustics are an option, but with these techniques it is difficult to measure the actual input force. Laser is only used when very small forces are needed. The most obvious technique to use is the impact hammer. An impact hammer is a semi-contact technique, the force can be measured accurately and the excitation location can easily be changed.

Excitation technique	**Contact/non-contact**	**Force range [N]**	**Excitation signal**	**Repeatability**
Electrodynamic shaker	contact	8-1800	arbitrary	fair
Hammer	contact	5-45000	impact	poor
Laser	non-contact	$< 5 \times 10^{-4}$	arbitrary	fair
Pressurized air	non-contact	$< 0{,}6$	impact	fair
Acoustics	non-contact	$< 5 \times 10^{-2}$	arbitrary	fair

Table 2: By comparing different excitation techniques, the hammer seems the most usable in practice [11]

However, impact testing mostly requires an experienced operator and definitely creates some issues to be dealt with. The experienced operator is needed to create a reproducible impact. Mainly, the location of the impact has to be reproduced, but also a reproducible force has benefits. The purpose of the measurement is mostly to fit a linear model on the data. If the amplitude varies, nonlinearities could be excited. Another

consideration is safety. Hitting a rotating shaft at high speed with a hammer could get the shaft unstable. Therefore, in this paper it is chosen to use an automatic impact system. The concept is shown in Figure 4. The hammer is fixed to a rotating point and will hit the shaft with a force depending on the starting angle Θ. To increase reproducibility and safety, the hammer is controlled by a stepping motor.The low signal to noise ratio due to the hammer impact [7] is reduced through averaging.

3.6 The test bench

A composition of the test bench is shown in Figure 5. It can be seen that it is possible to excite and measure the shaft at different locations. Also, the modularity allows other configurations such as different shaft lengths or addition of disks.

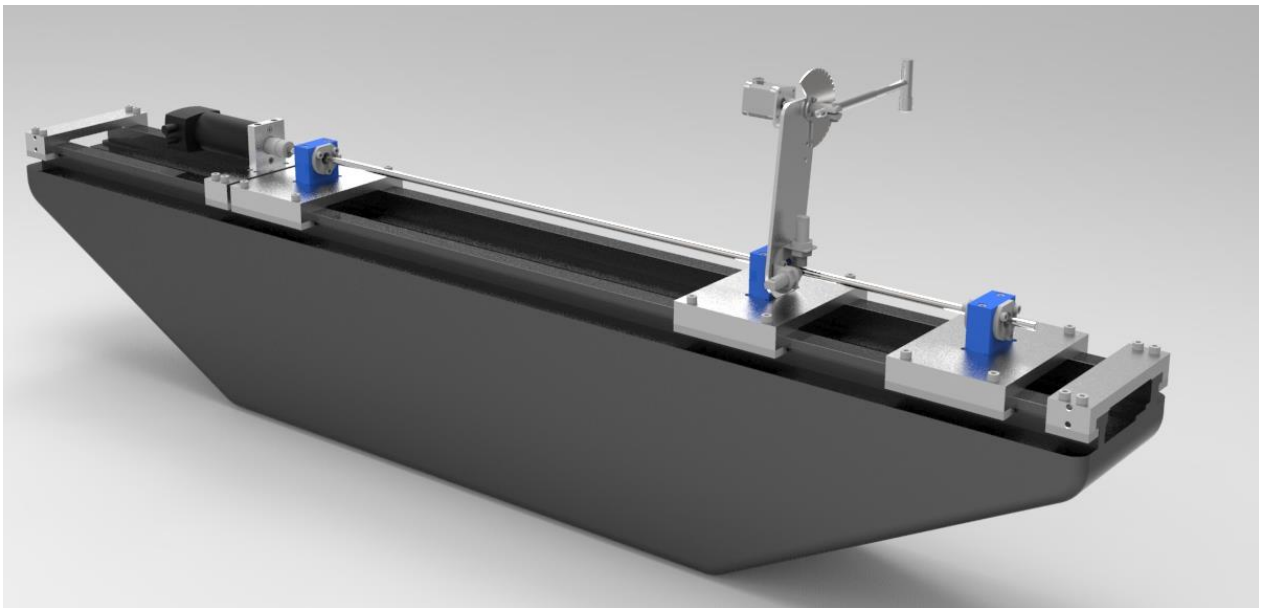

Figure 5: The test bench

4 The measurement procedure

4.1 Measuring the frequency response functions

The shaft is excited with the hammer and the responses are measured by eddy current probes. Eddy current probes typically generate a noisy signal and therefore every measurement is an average of 10 impacts. The frequency response functions are estimated with an H1 estimator [12].

4.2 Extraction of the poles

The poles are extracted with a least squares complex exponential method in time domain. The existence of forward and backward whirling in rotordynamics complicates the procedure. By hitting the structure with a hammer both whirling frequencies are excited. Because there is almost no gyroscopic effect present, forward and backward whirling frequencies coincide. Therefore, in the stabilization diagram, both poles corresponding to the forward and backward whirling can be found. Only poles corresponding to the forward whirling are important, because backward whirling is always stable. It is intended the poles corresponding to both forward and backward whirling.

Shaft diameter [m]	0,01
Shaft length [m]	1,115
Young modulus shaft [N/m^2]	2,2 $\times 10^{11}$
Density shaft [kg/m^3]	7730
Viscous damping factor shaft	2,30 $\times 10^{-5}$
Translational stiffness bearings [N/m]	3,5 $\times 10^{7}$
Rotational stiffness bearings [N/m]	300
Damping bearings [Ns/m]	2,3

Table 3: The parameters in the model are adjusted to fit the measurements

modeled		measured	
rad/s	rpm	rad/s	rpm
154,53	1475,65	153,94	1470,00
484,72	4628,73	497,00	4746,00
1023,82	9776,76	1030,44	9840,00

Table 4: The first three natural frequencies at standstill are practically the same in both model and measurements

4.3 Adjusting the model

In the construction of the model, there are still some parameters that are difficult to estimate. Mainly, the stiffness of the bearings in the housing, the damping of these bearings and the viscous damping factor of the shaft. These parameters are adjusted to fit the experimental data. The results are shown in Table 3 and 4.

5 Results

5.1 Frequency response functions

The frequency response functions in this paper are measured at one location on the shaft, 0,2 m from the bearings on the motor side (Figure 2). Both the excitation and the response are measured on this location. The resulting frequency response functions at 0 rpm and at 2500 rpm are shown in Figure 6 and 7. They are compared with the ones calculated directly from the model.

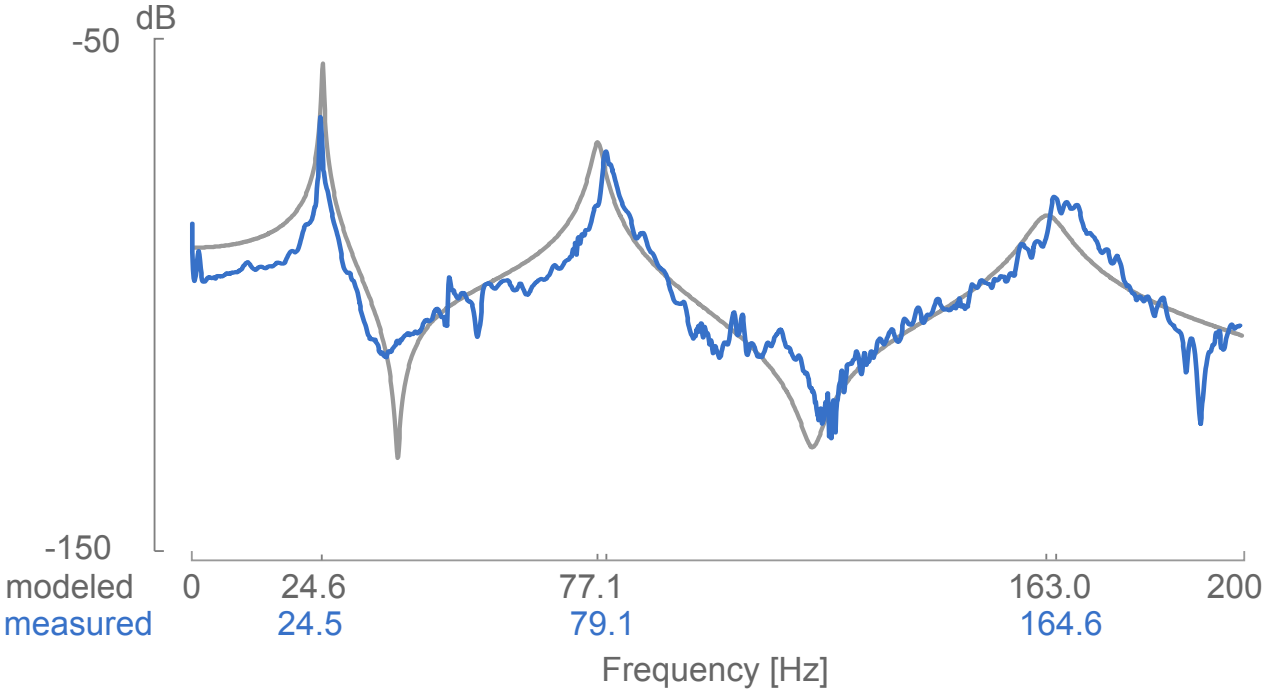

Figure 6: The frequency response function of the shaft at 0 rpm compared to the modeled one

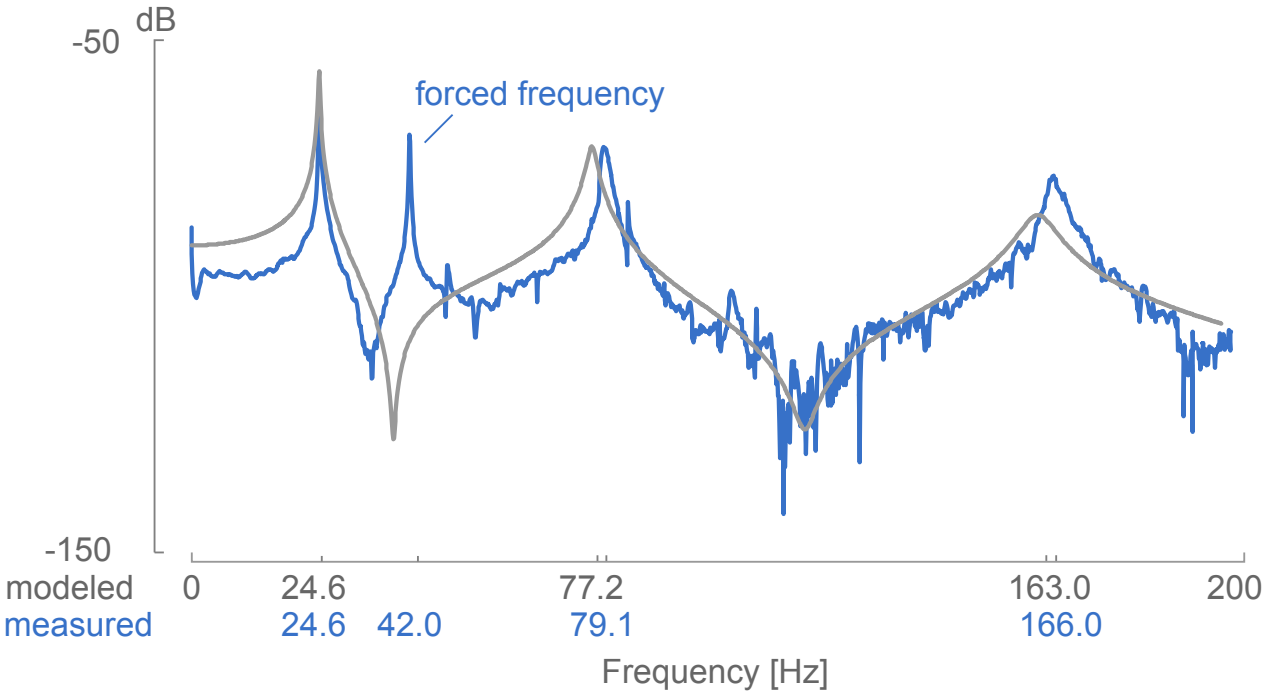

Figure 7: The frequency response function of the shaft at 2500 rpm compared to the modeled one

It can be seen that the measured frequency response functions correspond quite well to the ones calculated with the linear speed dependent model. There is one peak in the measurements that is not present in the model. This is the forced frequency caused by the shaft bow and coincides with the rotating frequency 2500 rpm or 41.6 Hz. It is important to remark that the speed dependency and linearity in the model correspond quite well based on these results. Visual inspection might suffice to decide if the natural frequencies coincide, it will not suffice to extract the influence of damping. Therefore, the poles are extracted from the FRF's.

5.2 Campbell diagram and decay rate plot

From the measured frequency response functions, the poles can be obtained. The poles can be splitted into their imaginary and real part and plotted in function of the rotating speed Ω, respectively called the Campbell diagram and the decay rate plot. For stability analysis, the decay rate plot is the most important, because it indicates when the system becomes instable. Figure 8 shows a comparison between the Campbell diagram as calculated from the model with the values extracted from the measurements. The different speeds at which the measurements where taken are shown on the graph. 500 rpm is lacking because the motor can not be controlled below 1000 rpm. At 1500 rpm, the rotating speed was to close to a natural frequency of the shaft (24,5 Hz) and it was not possible to take an FRF at this point. At 5000 rpm, the shaft has to cross the second natural frequency and it was decided not to do drive at this speed. Because the gyroscopic effect in this setup is very low, there is practically no influence by the rotating speed. Therefore, based upon this diagram, it can not be seen if the poles correspond to forward or backward whirling.

Figure 9 compares the decay rate plot from the model with the values extracted from the measurements. As reported in paragraph 4.2 it should be possible to find the poles corresponding to both forward and backward whirling. However, the graph shows that the poles are increasing in function of rotating speed, and based upon the theory, these poles correspond to the first forward whirling mode. The reason that the poles corresponding to the first backward whirling mode can not be found is still dubious. The absence of the poles corresponding to the backward whirling is likely caused by their fast decay in combination with the poorer signal to noise ratio.

When comparing the measured real parts of the poles to the ones calculated with the model, a similar trend is noticed. The model predicts that the rotor would be instable at 9195 rpm. By using linear regression on the measurement, one could decide the same for this stability threshold. The measured trend show some nonlinearity which can cause a stabilizing effect.

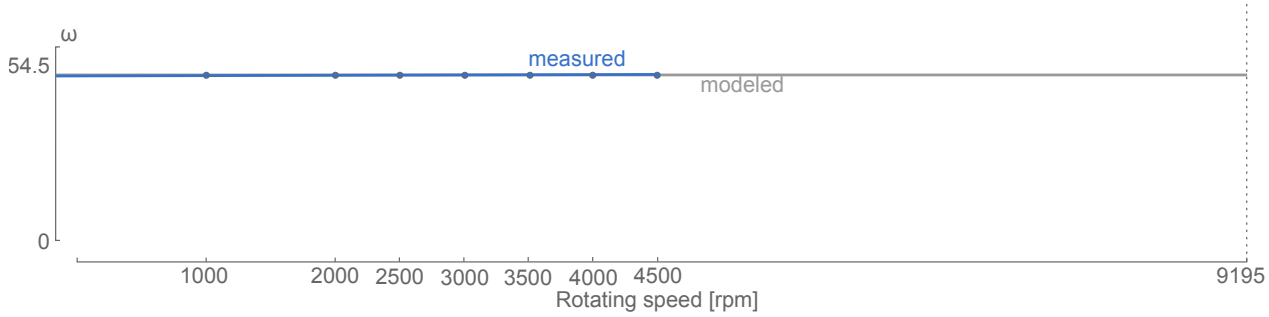

Figure 8: The measured and modeled Campbell diagram corresponding to the first (forward or backward) mode agree quite well

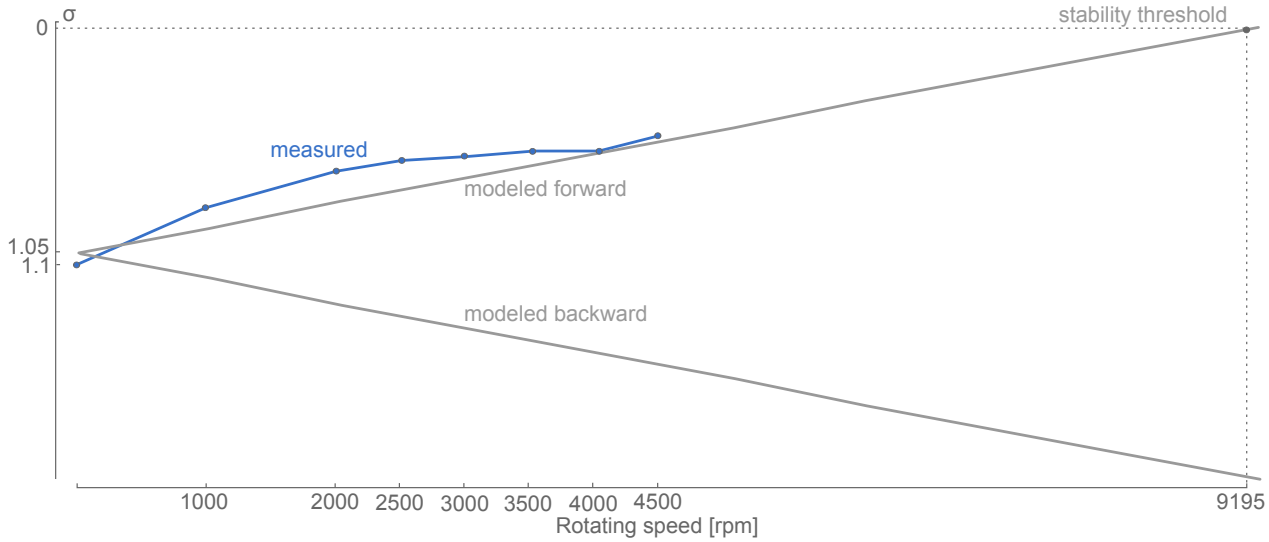

Figure 9: The measured and modeled decay rate plot corresponding to the first forward mode show the same increasing trend, but there seems to be an extra stabilizing effect in the measurement

6 Conclusion

In this paper the effect of rotating damping on the stability of rotors is discussed and experiments are used to validate the assumptions. By means of a linear speed dependent model, the stability threshold speed is derived and the parameters that affect this speed are discussed. In this model, the damping is chosen to be proportional to the stiffness. The damping in the bearings is proportional to the stiffness in the bearings, and the same holds for the shaft. Deviations are expected from this stability threshold speed because of the assumptions of linearity and the chosen damping type. In the experiment it is intended to create a rotating shaft that has clamped boundary conditions on both sides. Therefore the bearings and the housing play an important role. The boundary conditions of the resulting shaft lie somewhere inbetween clamped and pinned. An impact hammer is used to excite the shaft and eddy currents probes are used to measure the response. In order to create a safe and reproducible impact, an automated procedure is used. With this procedure it is possible to extract frequency response functions from the shaft while rotating. However, both an impact

hammer procedure and eddy current probes have a low signal to noise ratio, resulting in some noise on the FRF's. By looking at the frequency response functions only, the model and measurements fit quite well. It is difficult to draw conclusions about the damping from the FRF's only. Therefore, the poles are extracted form the FRF's at different rotating speeds and plotted in a Campbell diagram and a decay rate plot. It is seen that the Campbell diagram corresponds quite well. The decay rate plot shows a similar increasing trend, but seems to deflect leading to a possible more stable situation. In order to get a full explanation of this deflection, more measurements have to be performed. It should be noted that at this point it is not possible to find the poles corresponding to backward whirling modes. Because the test bench was chosen to have a negligible gyroscopic effect, the imaginary part of the poles coincide. In future research, a disk creating a gyroscopic effect can be used the split forward and backward modes and get a better view on the resulting poles.

References

[1] Maurice L. Adams, *Rotating machinery vibration: from analysis to troubleshooting*, CRC Press/Taylor & Francis, 2009.

[2] Anders Brandt, *Noise and Vibration Analysis: Signal Analysis and Experimental Procedures*, Wiley, 2011.

[3] I. Bucher and D. J. Ewins, *Modal analysis and testing of rotating structures*, Philosophical Transactions of the Royal Society A: Mathematical, Physical and Engineering Sciences **359** (2001), no. 1778, 61–96.

[4] L Forrai, *Instability due to internal damping of symmetrical rotor-bearing systems*, JCAM **1** (2000), no. 2, 137–147.

[5] Giancarlo Genta, *Dynamics of rotating systems, Volume 1*, Springer, 2005.

[6] Mohamed A Kandil, *On Rotor Internal Damping Instability*, Ph.D. thesis, 2004, p. 265.

[7] G. Ramanujam and C.W. Bert, *Whirling and stability of flywheel systems, part I: Derivation of combined and lumped parameter models*, Journal of Sound and Vibration **88** (1983), no. 3, 369–398.

[8] Françoise Tisseur and Karl Meerbergen, *The quadratic eigenvalue problem*, Society for Industrial and Applied Mathematics **43** (2006), no. 2, 235–286.

[9] B Vervisch, K Stockman, and M Loccufier, *Sensitivity of the stability threshold in linearized rotordynamics*, ISMA conference (Leuven), 2012.

[10] B. Vervisch, K. Stockman, and M. Loccufier, *Estimation of the damping matrix in rotating machinery for the calculation of the stability threshold speed*, International Journal of Structural Stability and Dynamics (2014), 1450012 (en).

[11] Bram Vervisch, Michael Monte, Kurt Stockman, and Mia Loccufier, *Acoustical Excitation for Damping Estimation in Rotating Machinery*, IMAC XXXI conference (Garden Grove), 2013.

[12] E. S. Zorzi and H. D. Nelson, *Finite Element Simulation of Rotor-Bearing Systems With Internal Damping*, Journal of Engineering for Power **99** (1977), no. 1, 71–76.